Design of slurries for 3D printing of sodium-ion battery electrodes

Reynolds, Carl D.; Alsofi, Giar; Yang, Junrui; Simmons, Mark J.H.; Kendrick, Emma

DOI:
10.1016/j.jmapro.2023.12.042

Document Version
Publisher's PDF, also known as Version of record

Citation for published version (Harvard):
Reynolds, CD, Alsofi, G, Yang, J, Simmons, MJH & Kendrick, E 2024, 'Design of slurries for 3D printing of sodium-ion battery electrodes', *Journal of Manufacturing Processes*, vol. 110, pp. 161-172. https://doi.org/10.1016/j.jmapro.2023.12.042

Journal of Manufacturing Processes 110 (2024) 161–172

Contents lists available at ScienceDirect

Journal of Manufacturing Processes

journal homepage: www.elsevier.com/locate/manpro

Design of slurries for 3D printing of sodium-ion battery electrodes

Carl D. Reynolds [a,c,*], Giar Alsofi [a,c], Junrui Yang [a,c], Mark J.H. Simmons [b,c], Emma Kendrick [a,c]

[a] School of Metallurgy and Materials, University of Birmingham, Elms Rd, Birmingham B15 2SE, United Kingdom
[b] School of Chemical Engineering, University of Birmingham, Birmingham B15 2TT, United Kingdom
[c] Faraday Institution, Quad One, Becquerel Avenue, Harwell Campus, Didcot OX11 0RA, United Kingdom

ARTICLE INFO

Keywords:
Battery electrodes
Sodium ion batteries
3D printing
Slurry rheology
Electrode coating

ABSTRACT

Additive manufacturing of battery electrodes, using syringe deposition 3D printing or direct ink writing methods, enables intricate microstructural design. This process differs from traditional blade or slot-die coating methods, necessitating tailored physical properties of composite slurries to ensure successful deposition. Inadequately optimised slurries result in non-uniform extrusion, and challenges such as nozzle swelling or slumping, result in compromised structural integrity of the print, limiting the resolution. This study focuses on developing slurry design principles by thoroughly characterising the rheology of several water-based hard carbon anode slurry, both in shear and extension. Hard carbon is chosen as a material of significant importance for future sodium-ion batteries, and an example for this optimisation. The slurry composition is tailored to introduce yield stress by incorporating network-forming binder (carrageenan) and additive (carbon nanotubes), effectively reducing spreading, and preserving the printed coating's structure. Validation is performed through printing a large width line and evaluating spread. The same slurry is deposited on a smaller 150 μm nozzle, which introduces die swell and spreading effects. This offers insights for further optimization strategies. The strategies developed in this research for characterizing and optimizing the rheology through formulation lay the groundwork for the advancement of detailed 3D printed electrodes, contributing to the progress of additive manufacturing technologies in the field of battery manufacturing.

1. Introduction

Manufacturing of battery electrodes is a highly topical issue, with demand for batteries predicted to require ten battery gigafactories in the UK alone by 2040 [1]. Electrodes are currently manufactured via a slurry casting process, industrially this uses a slot die coater, which produces a coating with uniform microstructure. The problems with scaling up this process lie with a lack of understanding of the underlying physics, which leads to optimisation by trial and error, giving high scrappage rates and long commissioning times [2]. Lithium-ion batteries are the current standard, but alternatives are sought due to issues with supply chain and sustainability of the critical materials involved [3]. One such technology is sodium-ion which uses much more abundant materials, and despite having lower energy density, with well optimised manufacturing can satisfy many of the use cases for lithium-ion [4,5]. Hard carbon anodes are the current state of the art for sodium batteries, but have difficulties with low initial coulombic efficiency which gives reduced energy density [6].

Structuring of electrode coatings has been researched for lithium-ion batteries and shown to be beneficial in decreasing the tortuosity of the coating, and thus increasing ion transport rates and allowing for faster charging. This strategy has been employed to produce thick coatings without loss of fast charging/discharging [7–9]. This enables thicker coatings with less inactive components (current collector and separator) which gives higher energy density in the final battery. This approach has been demonstrated to improve lifetime [10] and rate performance. It also enables faster wetting, It has been demonstrated that the 24 h wetting step can be removed for structured electrodes with 40–70 μm channels [11]. For sodium-ion batteries, these benefits could be useful in allowing the technology to compete with lithium despite overall lower energy density. Different structuring methods provide structure at different scales, small scale methods (e.g. templating [12]), can produce features on <10 μm scale but are difficult to scale to manufacturing. Zhu et al. provides a comprehensive comparison of current structuring methods [13]. Direct ink writing [14], which uses syringe deposition to 3D print electrodes is one of the most scalable methods of electrode structuring. It requires relatively simple setups, with low cost and can be performed at room temperature. The improved control over the coating

* Corresponding author at: Faraday Institution, Campus, Quad One Becquerel Avenue Harwell, Didcot OX11 0RA, United Kingdom.
E-mail address: c.d.reynolds@bham.ac.uk (C.D. Reynolds).

https://doi.org/10.1016/j.jmapro.2023.12.042
Received 7 August 2023; Received in revised form 9 November 2023; Accepted 19 December 2023
Available online 5 January 2024

uniformity leads to faster start-up times and means less electrodes need to be scrapped. Also, as the precise area of the electrode can be printed, it reduces waste in electrode offcuts [15,16]. Enabling precision in electrode design could also allow for design for disassembly approaches, improving rates of recovery at end of life [17]. This makes it a promising technology to integrate into sodium-ion battery manufacture, as the combined benefits for sustainability (reduction in critical materials, waste, energy required, recyclability) could be significant.

However, to scale this technique up, a precise understanding of the process is required, including the speeds attainable and the pressures needed to extrude material at the target thickness. There is also a limit to the size of structure attainable for electrode slurries (currently>100 μm). This is because small structure requires small nozzle sizes, which require low viscosity slurries to reduce pressure, which then spread on the surface losing the structure created. Hence optimisation of these slurries is key, the rheology or flow properties needs to be controlled, both in shear [18] and extension [19]. Fig. 1 shows an illustration of flow in a syringe, showing how shear is important to flow in the syringe and nozzle, and extension contributes to compression into the nozzle, and importantly, to the swell on leaving the nozzle, which can cause larger than desired features. Further spreading can occur once the slurry is deposited, which will be influenced by the rheology at low rates (i.e. under gravity), and the interfacial tension between the substrate and slurry. Integrated drying systems that dry the ink shortly after deposition have been proposed to reduce this spreading [20], but this adds complexity and may not be necessary with optimisation of the ink. In steady shear, optimisation targets high shear viscosity at low rates, which resists slumping, and low viscosity at high shear rates so that the slurry flows efficiently through the nozzle without excess build-up of pressure (Fig. 2) [21,22].

In addition, viscoelasticity is important, slurries ideally will have an elastic modulus, G′ greater than the viscous modulus, G″ at low strain amplitudes, indicating elastic behaviour which will resist settling of components and slumping under gravity. But the slurry also needs to flow, with G″ > G′ at higher amplitudes to allow flow through the nozzles [23]. The transition between these phases can be characterised by the yield stress, one way to measure this is using the crossover in G′ and G″ [24]. Finally, the timescales of these processes are important, the faster the slurry can relax after deformation, and recover the high viscosity and elastic behaviour, the less time it has to spread after coating.

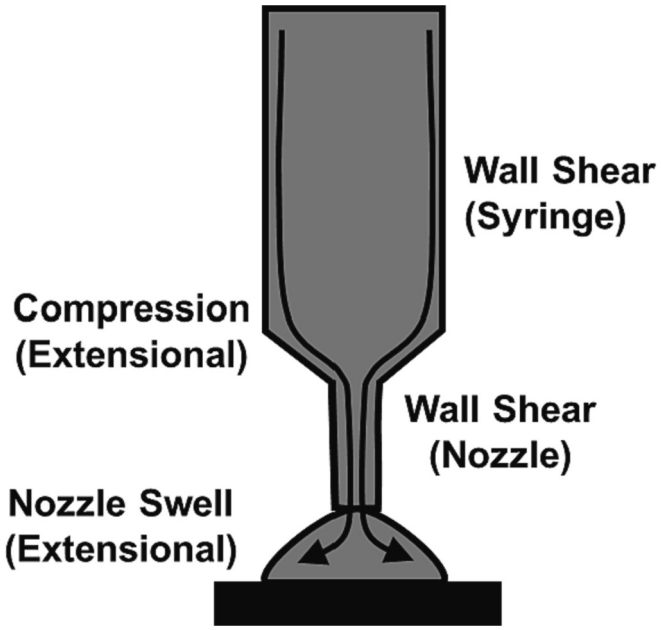

Fig. 1. Illustration of shear and extensional flow in syringe deposition.

Relationships for prediction of slumping in 3D printing have been proposed. M'Barki et al. [25] proposed an equation for the minimum yield stress, σ_y needed to prevent slumping in 3D printing of ceramics slurries:

$$\sigma_y \geq \frac{\gamma}{R} + \rho g h \quad (1)$$

Where γ is the surface tension, R is nozzle diameter, ρ is density, g is acceleration due to gravity and h is the nozzle height. This indicates the yield stress required is a balance between the capillary forces on the nozzles which cause spreading and gravitational slumping of the deposited line. Nelson and Ewoldt [26] have described design principles for the formulation of yield stress materials. Yield stress can be obtained through jammed systems with repulsive interactions (e.g. high particle loading suspensions) or networked morphologies with attractive interactions (e.g. colloidal gels).

This study optimises the rheology of a series of sodium-ion electrode slurry formulations, to achieve yield stress behaviour, high viscosity at low shear rates, and fast recovery time of viscosity after shear, as well as to understand the impact of different formulations on the rheology to allow for further optimisation. The methodology developed provides the design framework to optimise the slurry characteristics and printing parameters for direct ink writing.

2. Experimental

2.1. Materials

Hard Carbon was Kuraray Kuranode Type 2 (Average particle Size, D_{50} = 9 μm) . Carbon black was Imerys TIMCAL Super C65. Carboxy Methyl Cellulose (CMC) was Ashland BVH8. Styrene Butadiene Rubber (SBR) was Zeon BM451-B. Iota-Carrageenan was sourced from Fisher (AAJ6060322). Nanotubes were sourced from Nanocyl (Aquacyl AQ030X). Dispersant was Croda Hypermer Volt 4000, which is designed for dispersion of conductive carbon.

2.2. Slurry preparation

The formulation of solids in the slurry was (by weight percentage) 93:2:5 hard carbon: binder: carbon black. For CMC:SBR the ratio was 90:2:3:5 hard carbon: CMC: SBR: carbon black. The weight percentages and formulations are given in Table 1.

100 g of slurry was prepared using an Intertronics THINKY mixer. The binder (CMC, Carrageenan) was pre-dispersed in a stock solution at 3 % in water, mixing on a Silverson mixer overnight. Half of the binder solution was used to pre-disperse the carbon black, (with any additives, nanotubes or dispersant) and mixed for 1 min at 500 rpm, and 5 min at 2000 rpm. The hard carbon and final half of binder solution, with any additional water was added before undergoing a further mix for 1 min at 500 rpm, and 10 min at 2000 rpm mix and a degas step of 2200 rpm for 3 min. For CMC/SBR the SBR was added at the end before a final slower mix at 500 rpm for 5 min – the carrageenan slurries underwent this mix without addition to keep the procedure consistent. After mixing, the slurries are immediately taken for analysis and coating. Particle size was measured with three repeats of an Elcometer 2020 Hegman fines gauge. As a test of the 3D printability, an Osilla slot die coater was adapted to house a 1.5 mm nozzle, and a single line printed with a flow rate of 1.7 μl/s, a 1.5 mm height above the surface and a speed of 1 mm/s.

2.3. Rheology

Rheology was measured using a Netzsch Kinexus Pro+ rheometer equipped with a 40 mm roughened parallel plate, a roughened lower plate, and a measuring gap of 1 mm. Samples were loaded, and the gap was set to 1.05 mm. Samples were then trimmed, and the gap lowered to 1 mm to ensure there was no underfilling. Temperature was maintained at 25 °C using a Peltier plate and enclosure. Flow curves were performed

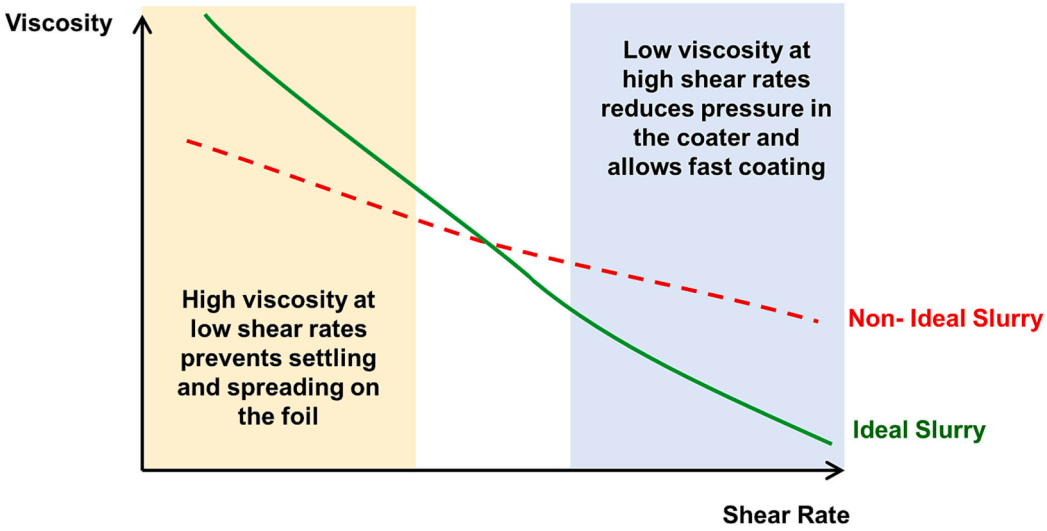

Fig. 2. Illustration of optimisation of flow curves for a 3D printed slurry, increasing the slope of the shear-thinning behaviour.

Table 1
Summary of formulations and physical parameters (HC = Hard Carbon, CMC = Carboxymethyl cellulose, I-C = iota-Carrageenan, SBR = Styrene Butadiene Rubber, Volt = Volt 4000 dispersant, NT = Nanotubes, CB = Carbon Black).

		Slurry						
		1	2	3	4	5	6	7
Wt% Component	HC	90	90	90	89	89	93	92
	CMC	2	2	2	2	2		
	I-C						2	2
	SBR	3	3	3	3	3	0	0
	Volt				1			
	NT					1		1
	CB	5	5	5	5	5	5	5
Solids Wt%		49.2	40	57.7	44.5	45.2	45	40
Slurry Hegman Gauge Particle Size (μm)		9 ± 1	9 ± 5	9 ± 10	5 ± 1	8 ± 4	5 ± 1	5 ± 1
Surface Tension (mN/m)		67 ± 2	48 ± 7	70 ± 10	48 ± 7	66 ± 7	*	*
Contact Angle on Al (°)		76 ± 6	71 ± 6	74 ± 8	71 ± 6	72 ± 4	*	*
Printed Line Width (mm)		2.2	1.6	1.9	2.3	1.5	1.5	N/A
Density (kg/m^3)		1240	1200	1290	1220	1230	1240	1210
Yield stress (Pa)		0	5.0	19.7	0.8	185	32.7	136
Extension Power Law Fit	Power Law Index, n	0.418	0.456	0.800	0.445	0.395	0.344	N/A
	Consistency Factor, K (N/m.s)	0.0113	0.0034	0.0309	0.0034	0.0084	0.0044	N/A

between 0.1 and 100 s^{-1} and equilibrium was deemed to be reached when the measured value was within 1 % for 10 s. Amplitude sweeps were performed between 0.01 % and 1000 % at 1 Hz. For the purposes of comparison, Frequency sweeps were then performed at a strain of 0.5 %, for a frequency range between 0.1 and 100 Hz. This was in LVE for all samples except the slurries 5–7. For these the LVE would have required <0.05 % and 0.5 % produced a less than two times change in G′. The range of some sweeps is smaller as the sample started to leave the gap at which point the test was stopped, and points in which the instrument had not reached steady state were discarded.

2.4. Surface properties

Surface tension measurements were conducted using a Dyne Sigma 703D tensiometer, using the Wilhelmy plate method. The plate was lowered just below the surface of the slurry, retracted and then the instrument zeroed. The plate was then lowered into the slurry and retracted so it was as close to the surface as possible, where the surface tension was allowed to stabilise, and recorded. This was repeated 3 times and averaged. Contact angle of slurry was measured on aluminium foil with an Osilla contact angle goniometer, on aluminium foil, an average of the left and right angles of two drops was taken as the contact angle.

2.5. Extensional rheology

The 3D printed Seymour extensional rheometer was used, with 1.9 mm top and bottom plates, as described by Reynolds et al. [19] The starting separation was 0.5 mm and final positions of the plates was 5 mm. The sample was loaded in between the plates and the solenoid switched on (producing a fast motion of the top plate, strike time of 0.005 s). This was imaged using a high-speed USB 3.0 camera, at ~ 500 fps. The filament diameters at the midpoint of the plates over time were extracted from the recorded videos using in-house MATLAB code.

2.6. Coating

A selected ink (Ink 7) was trailed for coating via draw down and 3D printing methods. The ink was coated onto carbon coated aluminium foil (20 μm) using a draw-down coater (K Paint applicator, RK Print-coat Instruments, UK) with an adjustable doctor blade. Coatings were dried on a hot plate at 50 °C and then at 120 °C in a vacuum oven overnight. The Automated Dispensing System, designed and manufactured by KWSP, was used for direct ink writing. Details of the system can be found in Gastol et al. [10] The slurry was deposited through a 150 μm nozzle, with a 100 μm height above the substrate. The movement speed was 7 mm/s with line spacing of 0.4 mm and a pressure on the syringe of 60

psi.

The coatings were imaged with a 5× lens using a Leica DCM8 microscope in focus variation mode. The lens was moved up and down and limits where no sample was in focus were found at each end, then a scan was performed between these two limits.

The coatings were cut with a scalpel and the edges imaged with a Carl Zeiss Sigma Field Emission Scanning Electron Microscope with an acceleration voltage of 20 kV and with an in-lens detector.

Confocal thickness profiles were performed with a micro-epsilon IFS2405–10 confocal sensor. The measurement was started on an area of bare foil to provide the zero and a Thorlabs LTS150 stage used to move the coating at 2 mm/s so the sensor measured across the coating. The 3D printed coating was measured perpendicular to the created lines, and the drawn down perpendicular to the direction of coating.

12 mm discs of the electrodes were cut from the centre of the coatings to measure the coatweight (from the mass minus the mass of current collector) and thickness measured using a dial gauge. 3 discs of each were measured and the coating thickness of the draw-down coating was 76 ± 2 μm, porosity 58 ± 1 %, and coat weight 50 ± 1 GSM, whereas the printed electrode was 72 ± 4 μm, 57 ± 1 % and 49 ± 3 GSM respectively.

3. Results and discussion

Table 2 lists the impact of slurry properties on three key processes in 3D printing, flow of the slurry through the nozzle, swell as the slurry leaves the nozzle, and slumping or spreading out of the slurry after deposition. Thus, we can define target properties for an ideal slurry, having steeply shear thinning behaviour with a rapid recovery of viscosity after shear in order to enable consistent flow through the nozzle and to retain the shape of the deposited inks. To alter the slurry properties, several strategies were trialled: changing the solids weight percentage, adding a network forming additive (carbon nanotubes), adding dispersant, and changing the binder system. The slurry formulation was modified from a baseline composition, with 90 wt% hard carbon, 5 wt% carbon black, 2 wt% CMC and 3 wt% SBR in water (49 wt% solids). The formulations were first assessed via rheology. Fig. 3 shows the viscosity curves for all the formulations. Changing weight percentage had relatively negative effects, increasing weight fraction did not have a significant impact on low shear viscosity, but introduced a peak at higher shear rates, due to particle-particle collisions, that increases the viscosity at the high shear rates relevant to direct ink writing. Decreasing weight fraction drops the viscosity at all shear rates.

Addition of dispersant also decreases viscosity at all shear rates, but slightly more so at low rates, suggesting better dispersion of agglomerates in the slurry, this is supported by the slightly smaller particle size observed in the Hegman gauge. While the impact on viscosity is counter to that required for direct ink writing, it should be noted that the reduction in particle size, is favourable for flow through small nozzles. Previous studies with graphite, required the use of specialist material with small particle sizes to reduce overall particle size and allow flow through the nozzle [10]. It is commonly quoted that particle size should be an order of magnitude lower than the extrusion gap (here the nozzle size) to avoid clogging, although a study of reinforced polymers found this limit at 6.2 [27]. Hence dispersants may form an important part of optimised formulations allowing the agglomerate size to get closer to the individual particle size [28,29] and allow flow through narrow nozzles.

Addition of nanotubes increased the low shear viscosity dramatically, attributed to increased formation of network structures that break up with shear. Changing the binder for iota-carrageenan had a similar effect, this is likely due to carrageenan's tendency to assemble into helical chains and form homogenous gels [30]. This self-assembled structure can be disrupted with shear but reforms as the slurry is allowed to relax. Because it introduces steep, uniformly shear thinning behaviour, designing electrode slurries using these attractive interactions appears to be a better strategy than increasing weight solids to create jammed structures, which is seen to lead to less steeply shear-thinning behaviour and higher viscosity at high shear rates.

As all slurries can flow through the nozzle, the high shear viscosity is not limiting the process for this system, thus the low shear viscosity is most important to optimise, and carrageenan and nanotubes show the most dramatic improvement.

From the oscillatory data, frequency sweeps (Fig. 4) and amplitude sweeps (Fig. 5), the slurries containing carrageenan, nanotubes and with high weight solids are the only ones that show significant elastic behaviour ($G' \gg G''$), required to resist settling of the components and slumping of coating on the foil. The high weight percentage slurry does however start to flow at higher frequencies and has a much lower magnitude of G' and G''. Strongly elastic behaviour, $G' > G''$ is preferred at low strains (e.g. under gravity) to resist flow of the slurry after 3D printing and for multi-layer printing, to support additional layers [31]. The nanotubes and carrageenan slurries show this most dramatically. A strain hardening peak is observed at high amplitude for many of the slurries, which has been previously been reported for graphite slurries in water, where it was attributed to particle-particle collisions, before which reaches a steady state with breakup of agglomerates at higher strains [18].

However, as well as elastic behaviour, a rapid return to elasticity after a high shear is needed, so that the coating does not slump before

Table 2
Slurry physical properties and their effect on the 3D printing process.

		Nozzle flow	Die swell	Slumping/spreading
Rheology	Viscosity at low shear rate	N/A	Magnitude of viscosity change related to amount of swell. Large change between high and low shear rates will likely swell more.	High viscosity slows slumping
	Viscosity at High shear rate	Low viscosity requires lower pressures and enables uniform flow from smaller nozzles		N/A
	Elastic / Viscous Modulus	Viscous must be greater than Elastic at high strains to allow flow	Elastic slurries more likely to swell	Elastic greater than viscous at low strains (independent of frequency) reduces slumping
	Recovery time	Short times reduce 'ooze' when flow stopped	Mostly effects the swelling profile, i.e. time taken to swell but not the magnitude of swelling	Fast gives less time to slump before viscosity recovered
	Extension	High extensional viscosity will increase pressure required	Highly elastic materials more likely to swell	High extensional viscosity may slightly resist slumping
	Yield Stress	Dictates the pressure required to achieve flow	Fast recovery of yield stress could impede swell	A significant yield stress resists slumping if recovery is fast enough
Surface Properties	Surface Tension Contact Angle	Small effect on the interface between walls and fluid, but effect of rheology is dominant.	Difference in interfacial properties between the nozzle and air may have small contribution but effect of rheology is dominant.	High surface tension and contact angle resists slumping on the foil, but also reduces capillary forces in the nozzle causing slumping.
Particle Size		Needs to be ~6-10× smaller than nozzle size to enable consistent flow	N/A – no direct effect but can impact rheology	N/A - no direct effect but can impact rheology

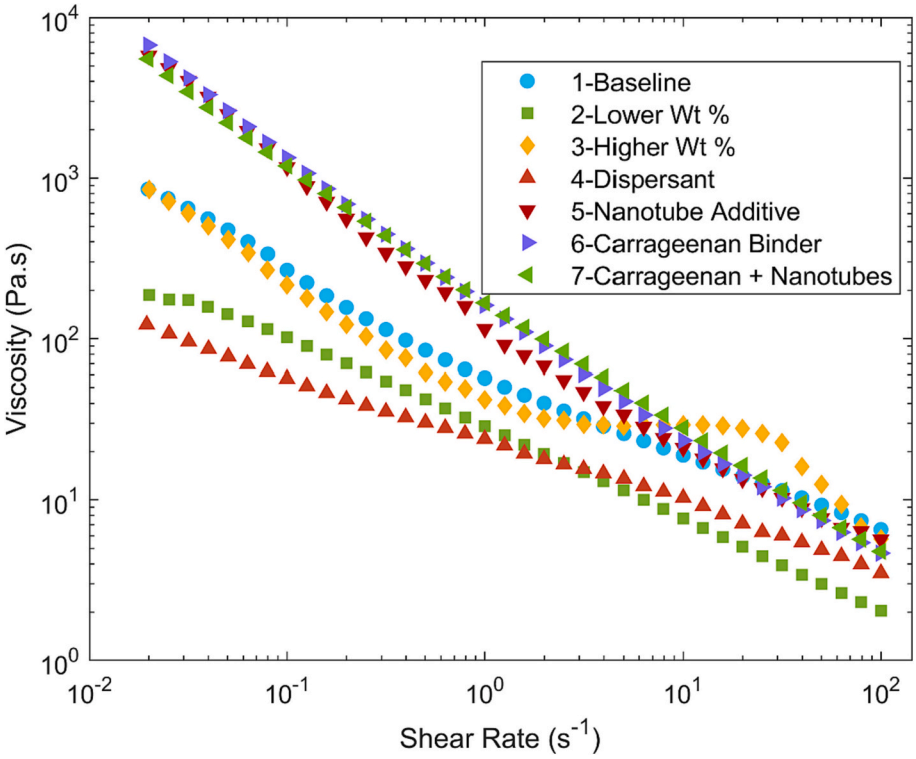

Fig. 3. Flow curves of all slurries.

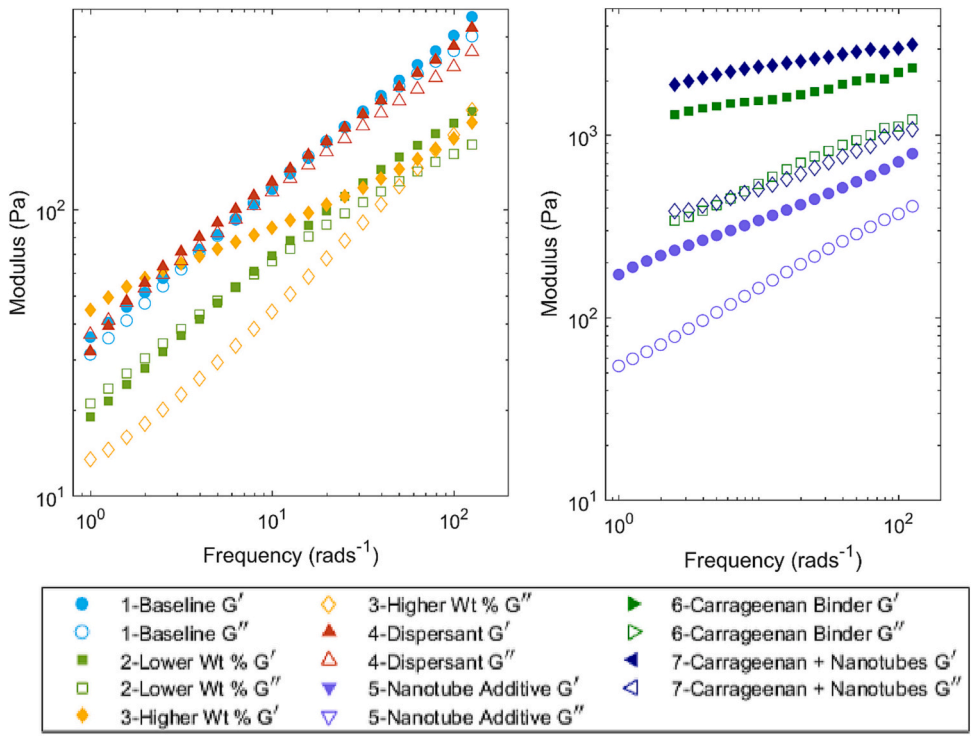

Fig. 4. Oscillatory frequency sweeps of slurries at 0.5 % strain.

the elastic behaviour has returned. Fig. 6 shows the viscosity trend for each slurry after a 60 s, 100 s^{-1} shear. Again, nanotubes and carrageenan show the most promise, with dramatic increases in viscosity, but the carrageenan containing slurry has the fastest response time, recovering completely in just fractions of a second.

The yield stress of the slurries (Table 1) was measured from the crossover in G′ and G″ during the amplitude sweeps, for all slurries except the baseline which began with G″ > G′ so did not demonstrate a yield stress. This indicates all of the formulation changes produced a yield stress; for the dispersant and low weight solids slurries, this is due to improved dispersion, which allows the components to better form a network throughout the slurry and avoid agglomeration, allowing the

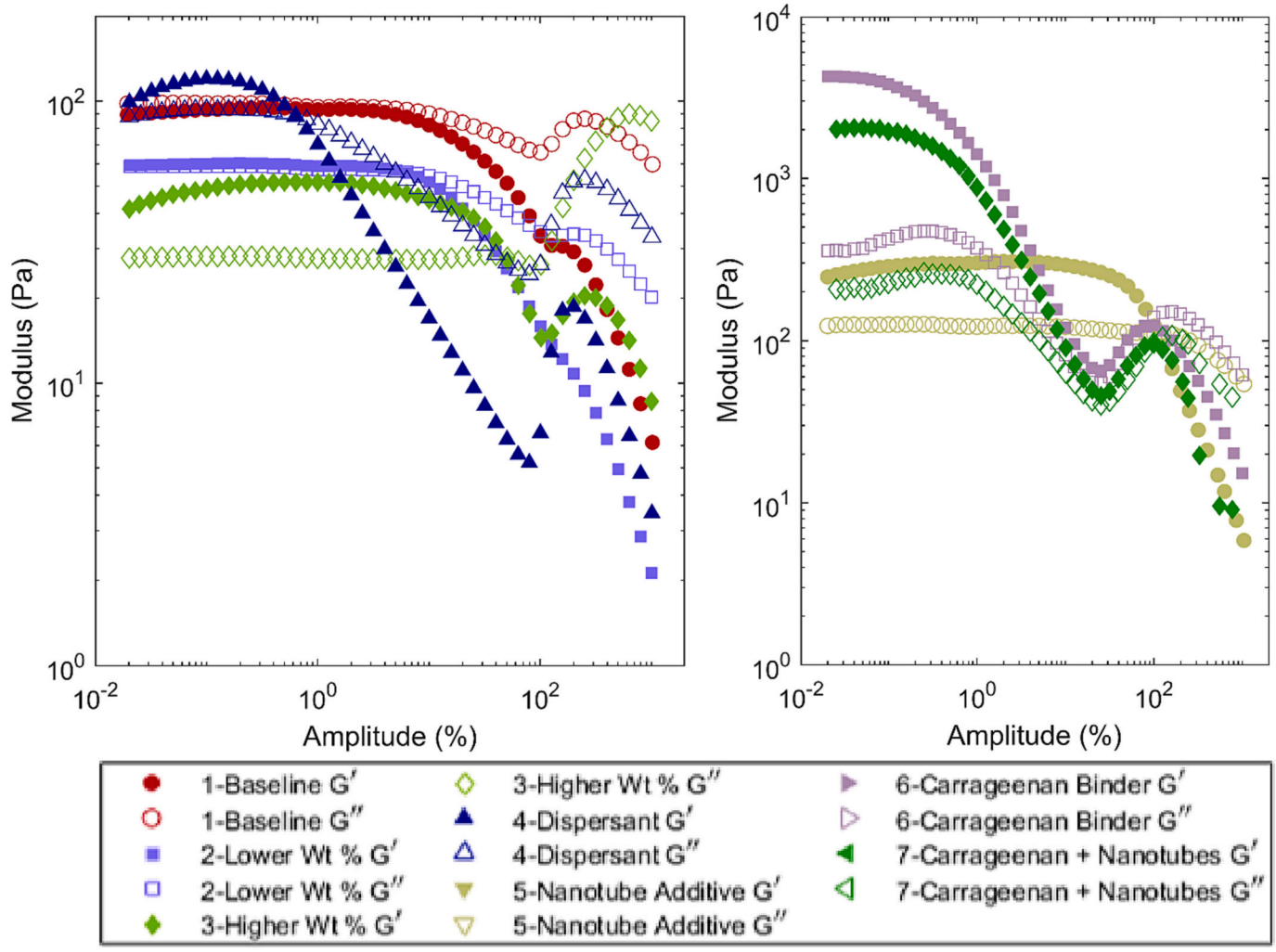

Fig. 5. Oscillatory amplitude sweeps at a frequency of 1.

crossover into weakly elastic behaviour. For the increase in weight solids, this is due to the creation of a network of repulsive particle-particle interactions, whereas for the nanotubes and carrageenan, attractive colloidal interactions provide the yield stress.

Eq. (1) predicts that a value of ~40 Pa is needed for all our slurries to prevent settling in the test setup with a 1.5 mm nozzle, which only slurry 6 and 7 exceed. However, moving to the 150 μm nozzle to be used in the 3D printer, this rises to ~400 Pa, which none of the slurries exceed. Hence there may be scope for further optimisation to bring additional increases in yield stress. This likely can be achieved by increasing the overall weight solids of the slurries, which were lower than the baseline for carrageenan and nanotube containing slurries due to difficulties in mixing. Switching to a more intensive mixing process than the planetary mixer would likely alleviate these problems and allow the yield stress to be further increased. Alternatively, higher fraction of binder or nanotubes would also be possible routes to a higher yield stress.

As well as rheology, surface properties were considered. The surface tension for all slurries is given in Table 1, but was not possible to ascertain for the nanotube and carrageenan slurries due to their high viscosity and elasticity causing too much force on the Wilhelmy plate. The slurries which showed a significant difference in surface tension were the low weight fraction and the dispersant, which both showed lower surface tension. In the case of the dispersant this is expected, as the dispersant molecules, as well as stabilising particle interfaces, also reduce the energy of the solvent-air interface. For the low weight solids slurry, the reason for the lower value is likely due to better dispersion at lower solids loading [32] leading to a better mix of components at the slurry-air interface. The differences in contact angle on aluminium were within the error between the formulations, despite the differences in surface tension, again the contact angle of the carrageenan slurry was not possible to ascertain due to its high elasticity meaning it retained the shape it was applied to the foil and did not relax into a drop; however, this does suggests promise for shape retention in 3D printing.

There were only two significant differences in the Hegman Gauge particle size, the inclusion of Volt 4000 additive gave a slight reduction, likely due to improved dispersion of agglomerates. Dispersants will aid direct ink writing as the particle sizes need to be as small as possible to allow efficient flow through the nozzle. However, they also commonly have the effect of lowering surface tension, which causes slurry to spread on the current collector, and makes maintaining fine structure more difficult. The carrageenan slurries also gave a slight reduction in particle size, this could be due to the lower weight solids, combined with higher viscosity, which will improve dispersion in the planetary mixer. The error in this value can give us insight into the uniformity of the slurry. The error in the high weight fraction slurry was high, suggesting an uneven distribution with some larger agglomerates, which may indicate the weight fraction is too high to mix efficiently, or that settling is occurring after mixing.

To evaluate the slurries for 3D printing accuracy, a single line was printed using a large 1.5 mm nozzle, so the differences in line thickness could be easily captured optically. Fig. 7 shows the setup used for this test alongside two lines of different widths resulting from printing. All

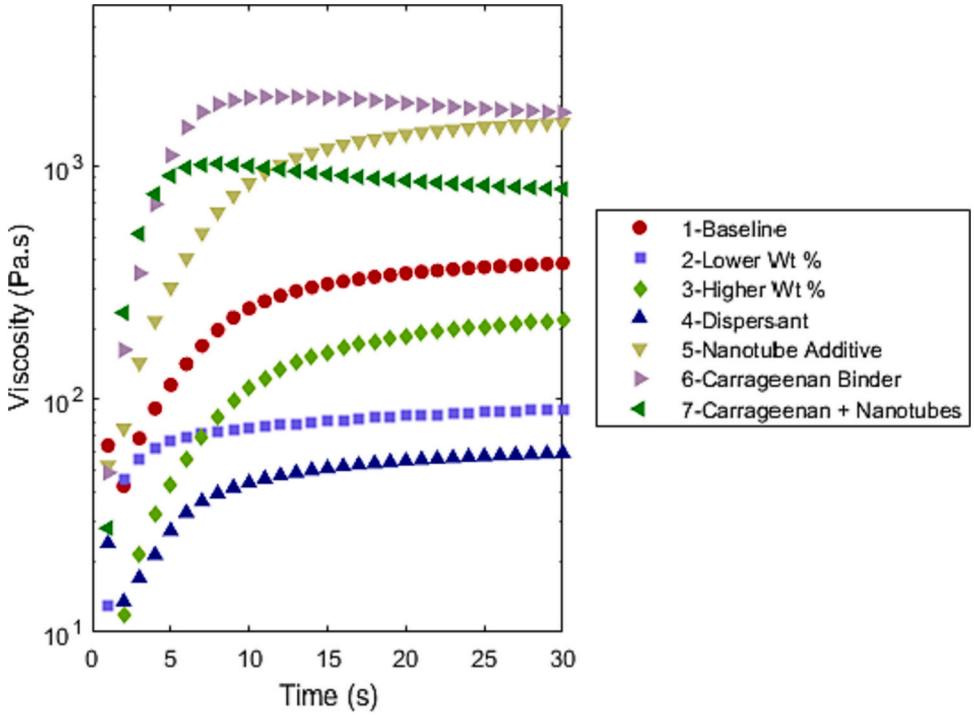

Fig. 6. Recovery of viscosity after a 60 s, 100 s^{-1} shear.

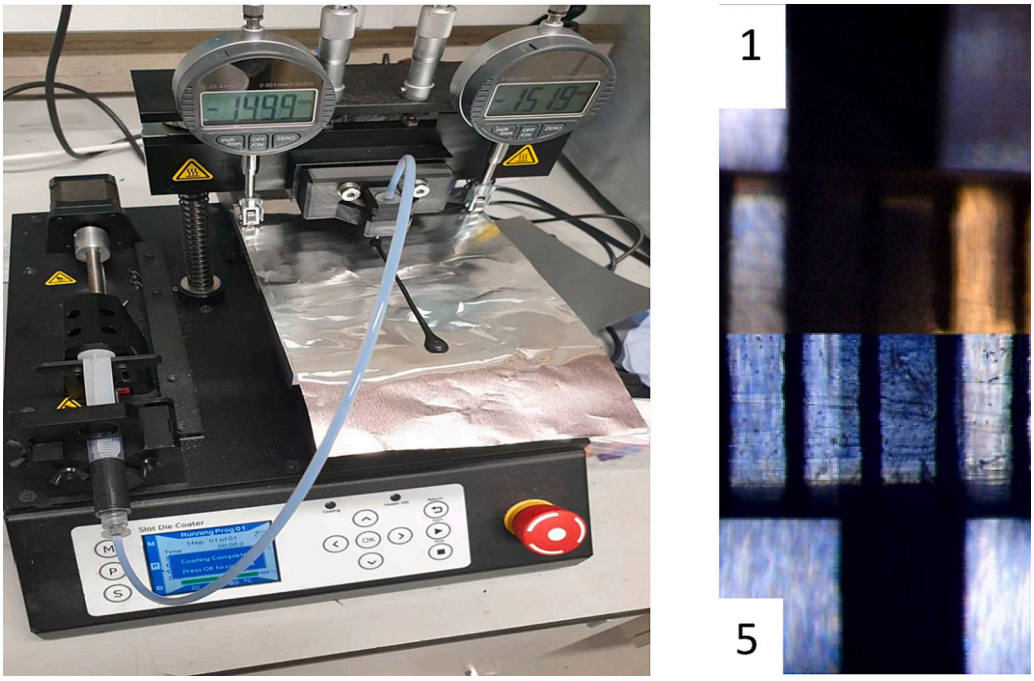

Fig. 7. Setup for printing a test line (left) with example results (right), showing the difference in thickness between the baseline slurry (1) and the nanotube containing slurry (5), each mark represents 0.1 mm. Measured thickness values are given in Table 1.

the line widths are given in Table 1. From the results of the 1.5 mm printed lines, the initial slurry showed significant slumping, giving a ~ 70 % wider line than printed. The only formulation with a higher value was the slurry with dispersant, which spread slightly more. This is due to the lower surface tension and contact angle which would be expected to increase spreading on the foil, and thus increase the width of 3D printed features. However, surface tension also increases the capillary forces, which increases the yield stress required to prevent spreading via Eq. (1). At a nozzle size of 1.5 mm, surface tension provides a relatively small change in the required yield stress (a 30 mN/m changes gives a change of 20 Pa), hence this did not impact the printing.

The result from the lower weight solids slurry (slurry 2), was unexpected. It provided a much thinner printed line than the original slurry, despite decreasing the viscosity which may be expected to increase spreading. However, it also demonstrated a small yield stress, and had one of the faster recoveries after shear, both of which will impede the

slurry spreading. This suggests the presence of a structured network within the slurry, which may be due to the lower weight solids increasing the efficiency of the planetary mixing and reducing the occurrence of agglomeration. This is supported by the very small yield stress obtained for the dispersant containing slurry, which also is expected to have improved dispersion.

The results for the other slurries are in-line with predictions, where the increased viscosity and presence of a yield stress impedes spreading and provides thinner 3D printed lines than the original formulation. Because no discernible change in contact angle on the Al foil was observed, it was determined for these formulation changes, the surface properties did not vary enough to give large changes in the printability, and the performance improvements would be achieved through rheological optimisation.

Eq. (1) predicts all slurries with a yield stress of ~40 Pa would be able to resist slumping at this nozzle size, and this correlates well with the thickness of the printed line, although the carrageenan slurry 6, had a slightly lower value than this limit but did not demonstrate spreading. Thus, this approach is a useful estimate of the spreading potential of the slurries. However, the timescales of this process are also important, so in addition to a yield stress, the slurry needs a rapid recovery of elastic behaviour after deformation. The carrageenan and nanotube containing slurries had the fastest recovery times, and also performed best in the 3D print test.

In the extensional tests (Fig. 8), all the slurries were fitted with a power law decay [19], which fit the curves well. The only notable difference in shape is for the higher weight fraction, where a plateau is noted at long times, likely due to particle collisions. This may pose issues for compression of the sample through the small nozzle. The decrease in extensional time to breakup correlates well with the decrease in recovery time seen in shear because a rapid return to elastic behaviour after deformation promotes a rapid breakup of the filament. There do not appear to be notably different drivers for shear and extension for these slurries, but care must be taken when adding network forming components, as networks often lend increases in extensional viscosity which are above those in shear [33,34], which can cause high pressures and die swell. However, these seemingly breakup under both shear and extension and so the overall drivers for both modes of rheology are similar. Note that in previous studies [19] carrageenan gave a slightly longer extension time than CMC but there both CMC and SBR were replaced with carrageenan so the overall weight percentage of dissolved binder (CMC or carrageenan) was higher for the carrageenan slurries than the CMC.

A summary of the impact of formulation on the slurry properties required is given in Table 3.

3.1. Coating and 3D printing

From the formulations tested, a final slurry with both nanotubes and carrageenan was selected to assess printability on a smaller nozzle. Because of the large increases in viscosity from both additions, the weight fraction had to be reduced slightly to 40 %, to enable efficient mixing in the planetary mixer. However, mixing at higher weight fractions would likely be possible with more intensive mixers. Dispersant was not included because the agglomerate size of all slurries was small (≪nozzle size), but for other materials with larger particle sizes e.g. graphite, this reduction in agglomerate size may be key.

The selected slurry was printed through a 150 μm nozzle with a spacing of 0.4 mm between printed lines. The nozzle size is close to the smallest size possible given the hard carbon particle size of 9 μm, and . This spacing was selected from trials to give some visible structure but no areas of bare uncoated foil. From this value, it is clear that the results on the 1.5 mm nozzle do not translate to the nozzle an order of magnitude smaller. Because if a 150 μm was printed with zero spreading, any spacing above 0.15 mm would give areas of uncoated foil. There are two potential reasons for this. One is the yield stress, using Eq. (1), decreasing the nozzle size brings the required yield stress up to ~400 Pa, which is above the yield stress of the slurry. Therefore there may be spreading of the slurry at this size. It is also possible the reduction in nozzle size increased the contribution of elasticity and die swell, and the slurry swelled due to the high elasticity observed.

Optical images of the coating produced are shown in Fig. 9, with a draw down doctor blade coating shown for comparison. Fig. 10 shows thickness profiles across each coating from a confocal sensor scanned across the coating. A feature of the 3D printer motion leads to lines not being equally spaced, but each pair of lines being slightly closer together, with a larger gap before the next pair, this leads to a more significant undulation every 0.8 mm and a smaller one every 0.4 mm. The images demonstrate that the 3D print is actually more uniform than the draw down coating, which shows large variations with a thin section neat the coat edge. This highlights the need for care when taking small samples of draw down coatings for coin cell testing. The 3D print does however demonstrate the targeted localised undulations, of around 20 μm between 80 and 100 μm. The spacing, as seen in the microscopy, is every 0.4 mm, but each pair has merged, giving the largest variation every 0.8 mm with a smaller ~10 μm undulation in between.

It is possible that the 3D printing technique could lead to differences in microstructure of the electrodes (e.g. shear alignment), however the SEM images (Fig. 11), show no noticeable structural differences between the draw down and 3D printed electrodes.

In order to understand the 3D printed results further, it is useful to

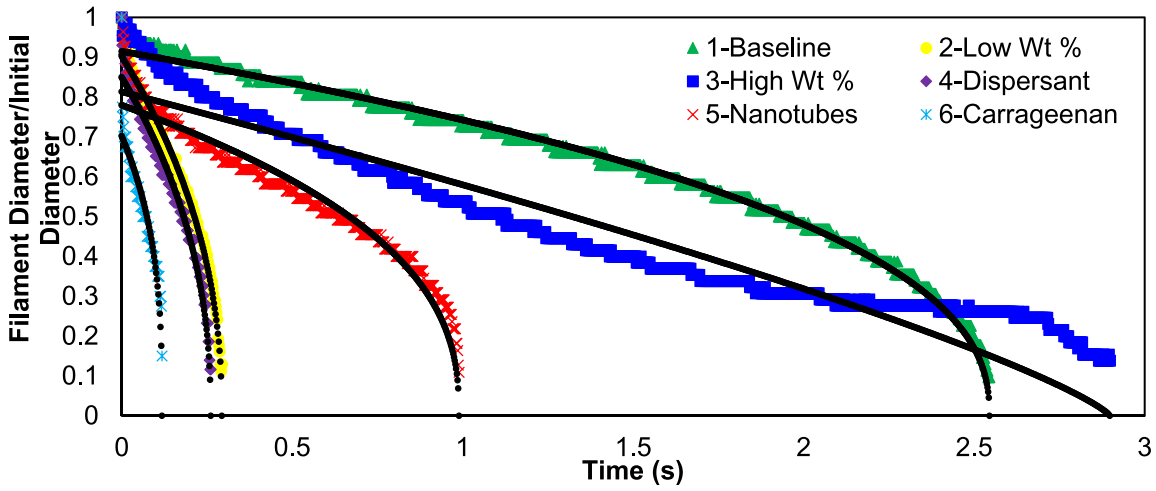

Fig. 8. Decay of filament diameter measured using the Seymour extensional rheometer, with power law fits shown in black.

Table 3
Impact of formulation on slurry physical properties.

		Weight solids	Nanotube additive	Binder	Dispersant
Rheology	Viscosity	Increasing weight solids increases viscosity uniformly, but can lead to settling/agglomeration and particle jamming leading to hardening at high shear rates	Additives which form networks which break up with shear, like carbon nanotubes, lead to significant viscosity increases at low shear rates	Alternative binders can significantly modify the viscosity profile. Iota-carrageenan increases viscosity over CMC, particularly at low shear rates.	Reduces viscosity, particularly at low shear rates, due to dispersion of weakly bound agglomerates
	Elastic / Viscous Modulus	High Weight solids introduces elastic behaviour but flows at high frequency	Elastic greater than viscous at low strains reduces slumping	Elastic slurries more likely to swell	Flows at most frequencies, with large reduction in strain required to induce flow
	Recovery time	Lowering weight solids gives faster recovery but smaller magnitude of change	NT induced fast change in viscosity on stopping shear, but full recovery slow	Carrageenan binder induces very fast change recovery	Little change to rate of recovery, reduces magnitude of change
	Extension	Increasing weight percentage increases time to breakup and changes profile	Reduction in extensional time to breakup	Largest reduction in extension time to breakup	Significant reduction in time to breakup
	Yield Stress	Introduces yield stress	Introduces yield stress	Introduces yield stress	Introduces small yield stress
Surface Properties		Reduced weight fraction decreases surface tension, possible due to better dispersion at the interface	Has little impact on surface tension	N/A- Change in rheology made surface properties difficult to obtain	Dispersant reduces surface tension in a similar way to reducing weight fraction
Particle Size		No observable change but large erroring high weight solids slurry suggests some large agglomerates	No change	Alternative binder reduces particle size, possibly due to increased viscosity improving mixing	Reduction in particle size

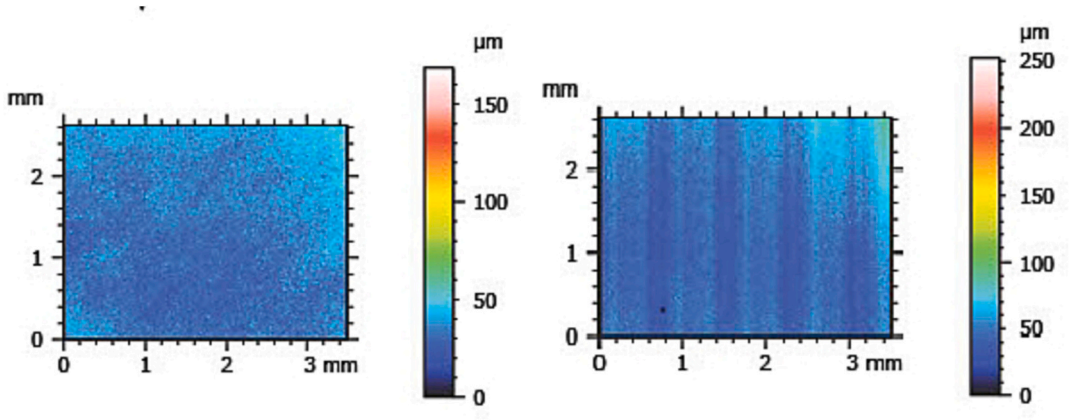

Fig. 9. a)5× optical microscope image of draw down coating, b) 5× optical image of the 3D printed coating.

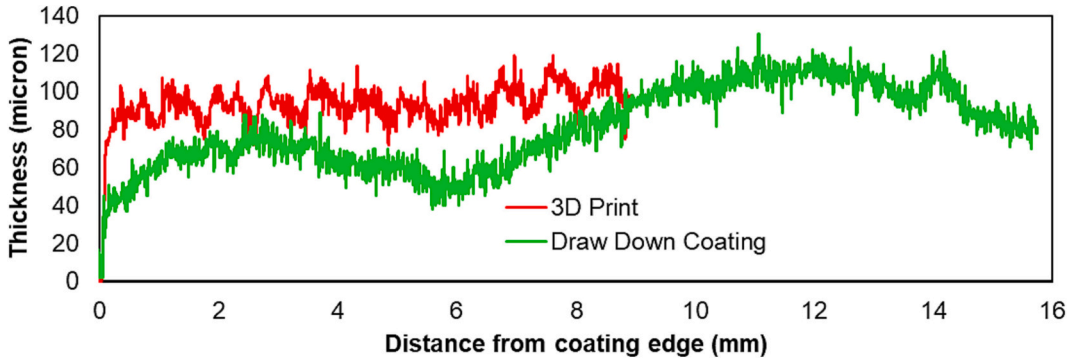

Fig. 10. Confocal thickness profiles for the draw down and 3D printed coating. Note 0 thickness corresponds to bare foil.

extract a shear rate in the nozzle. However, this is not simple because a fixed pressure is applied to the syringe, rather than dispensing at a fixed flow rate. A volumetric driven printer is desirable to easily extract shear rates for comparison to the rheology and subsequent optimisation. However, for pressure driven printers the shear rate can be estimated from the mass of the coating produced. First the volumetric flow rate, Q, is calculated, using

$$Q = \frac{\frac{m}{\rho^* x}}{\nu^* \frac{A}{2^* w}} \quad (2)$$

where m is the mass of dry coating, ρ is the density of the slurry, x is the weight fraction of the slurry, ν is the coating speed, A is the coating area and w is the line separation. The Rabinowitsch corrected shear rate (for shear thinning fluids) [35] then can be calculated using:

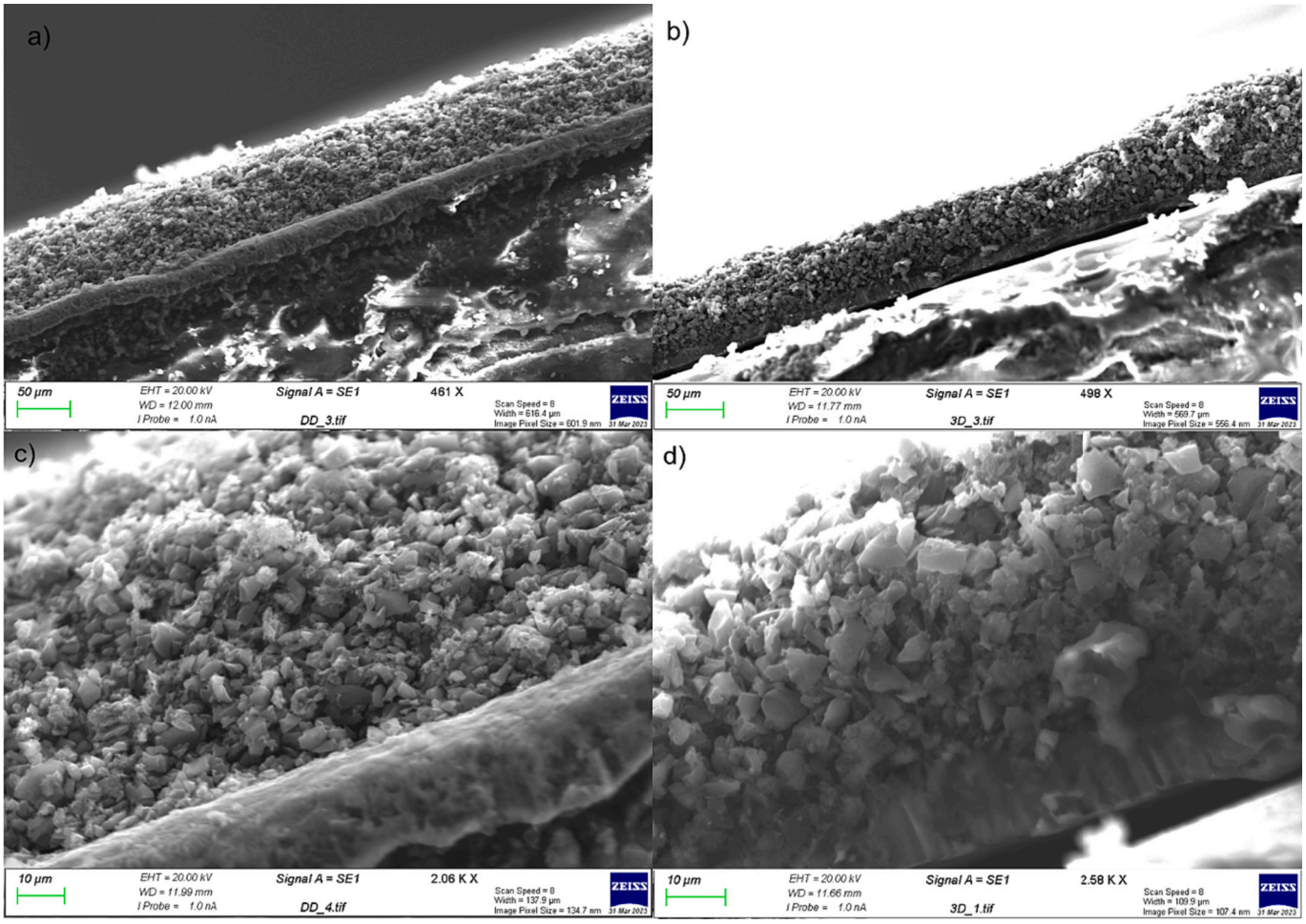

Fig. 11. SEM Images of: a), c) a cut 3D printed electrode, b), d) a cut Draw Down electrode.

$$\dot{\gamma} = \frac{(3n+1)}{4n} * \frac{4Q}{\pi R^3} \tag{3}$$

Where n is the power law coefficient obtained by fitting a power law, $\eta = K\dot{\gamma}^{n-1}$ to the viscosity data, giving K = 70.96 and $n = 0.435$ for the final slurry 7.

This gave a shear rate of 280 s^{-1} for the 3D printing. This is relatively high, especially when compared to the shear rate required to exceed the yield stress for the slurry, which is two orders of magnitude lower (Fig. 12). This means there is significant scope for reduction of the printing pressure to improve the detail of the structure obtained, however this requires care because other factors may make such pressures

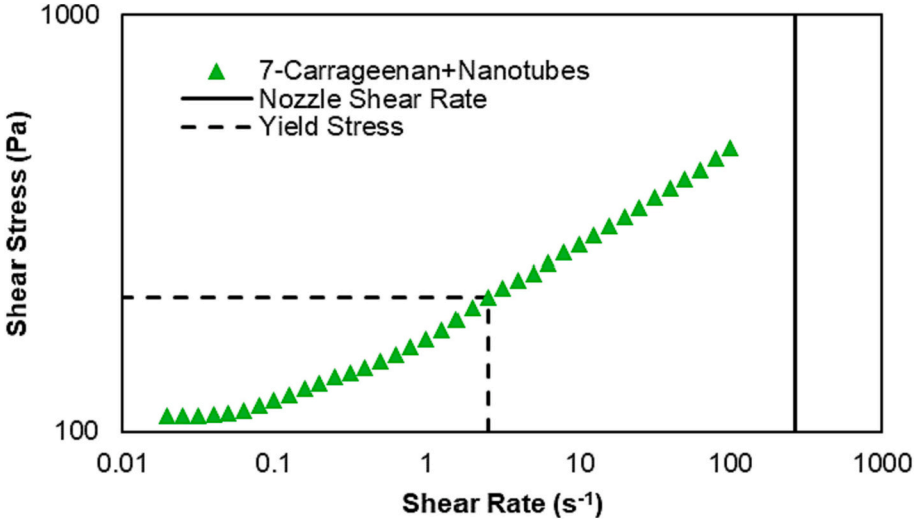

Fig. 12. Flow curve for the 3D printed slurry, showing the yield stress and nozzle shear rate.

unfeasible. For example, if drying of the slurry occurs in dead zones when the flow rate is too low.

The coating effectively demonstrated efficient printing from a small nozzle, creating a uniform coating of precise size, with features of ~20 μm. The 3D printed coating was more uniform than a draw down coating, with a similar porosity and coatweight in a single layer. However, the ability to create non-uniform structures was hindered by die swell and spreading at this nozzle size, and we have also noted that to achieve a higher structural resolution from very small nozzles, more intensive mixing is required to produce slurries with higher weight solids and network forming additive content, which in turn will have high enough yield stress to resist spreading. The use of more intensive mixers to achieve this rheology and thus further increase printing resolution, will be the focus of future work.

4. Conclusions

3D printing such as direct ink writing is a scalable method for electrode structuring, offering improved control over coating uniformity and reduced waste. The rheological properties of electrode slurries play a crucial role in the 3D printing process for electrode manufacturing. Here we provide formulation options for electrode slurries through direct ink writing. The process differs significantly from blade or slot die coating and the physical properties of the slurry require optimisation. To do this a set of target properties needs to be established, as well as an understanding of how these can be achieved via formulation, which are proposed here. We also demonstrate how shear rates can be extracted which are required for further optimisation, although note that a volumetric driven printer simplifies extraction of shear rates and thus optimisation. Finally, the optimisation for a large (1.5 mm) nozzle, is shown not to fully translate to a smaller 150 μm nozzle, which requires higher yield stress and reduced elasticity to prevent die swell. A summary of the key design rules:

- The optimisation of electrode slurries for 3D printing is dependent on factors such as viscosity at relevant shear rates, yield stress, and viscoelasticity of the slurry.
- Both shear and extensional forces must be considered, ideal slurries have a rapid return to high viscosity under shear and extension to allow consistent flow through the nozzle and reduce swell. While the drivers for both can be the same, for some materials e.g. branched polymeric binders, the behaviour in shear and extension can differ significantly [19].
- The presence of a yield stress in the slurry resists slumping to provide resolution in the print as well as settling in the slurry. The yield stress must exceed both capillary and gravitational forces to obtain printing resolution close to the nozzle size, as quantified by the 3D printability dimensionless number of M'Barki et al. [25]
- The rheology is dominant over the surface properties of the slurry but at smaller nozzle sizes capillary forces become more important and reduction in surface tension can reduce spreading.
- Yield stress is not the only driver of slumping, and a rapid recovery time after deformation, in shear and extension, is required to prevent spreading of the 3D printed coating.
- Increasing the weight percentage of particulate materials in the slurry leads to a significant reduction in the recovery time after shear and an increase in extensional time to breakup.
- Network forming additives and binders, nanotubes and carrageenan binder, produce yield stress in the slurry.
- Dispersant decreases agglomerate size, important to enable smooth flow for systems where the agglomerate size is of the same order of magnitude as the nozzle diameter.

Understanding and optimizing the rheological properties of electrode slurries is crucial for achieving improved performance and sustainability in electrode coatings. This study provides strategies for the design of hard carbon anodes for 3D printing, which is required to achieve improved performance and sustainability of electrode coatings, and to combine with internal structuring of the electrodes to allow for multi-level design.

Funding

This work was supported by the Faraday Institution NEXTRODE project (faraday.ac.uk; EP/S003053/1, FIRG015).

Declaration of competing interest

The authors declare the following financial interests/personal relationships which may be considered as potential competing interests: Carl Reynolds reports financial support was provided by The Faraday Institution. Emma Kendrick reports financial support was provided by The Faraday Institution. Mark Simmons reports financial support was provided by The Faraday Institution.

Data availability

The raw/processed data required to reproduce these findings cannot be shared at this time as the data also forms part of an ongoing study.

References

[1] UK Electric Vehicle and Battery Production Potential to 2040. UK Electric Vehicle and Battery Production Potential to 2040 – Update Published June 2022. The Faraday Institution. https://www.faraday.ac.uk/ev-economics-study-2022/ (accessed 2023-03-20).
[2] Reynolds CD, Slater PR, Hare SD, Simmons MJH, Kendrick E. A review of metrology in lithium-ion electrode coating processes. Mater Des 2021;209:109971. https://doi.org/10.1016/j.matdes.2021.109971.
[3] Lebrouhi BE, Baghi S, Lamrani B, Schall E, Kousksou T. Critical materials for electrical energy storage: Li-ion batteries. J Energy Storage 2022;55:105471. https://doi.org/10.1016/j.est.2022.105471.
[4] Rudola A, Sayers R, Wright CJ, Barker J. Opportunities for moderate-range electric vehicles using sustainable sodium-ion batteries. Nat Energy 2023;8(3):215–8. https://doi.org/10.1038/s41560-023-01215-w.
[5] Usiskin R, Lu Y, Popovic J, Law M, Balaya P, Hu Y-S, et al. Fundamentals, status and promise of sodium-based batteries. Nat Rev Mater 2021;6(11):1020–35. https://doi.org/10.1038/s41578-021-00324-w.
[6] Recent advances in hard carbon anodes with high initial Coulombic efficiency for sodium-ion batteries - ScienceDirect. https://www.sciencedirect.com/science/article/pii/S2589965122000058 (accessed 2023-03-26).
[7] Wang Z, Dai C, Chen K, Wang Y, Liu Q, Liu Y, et al. Perspectives on strategies and techniques for building robust thick electrodes for lithium-ion batteries. J Power Sources 2022;551:232176. https://doi.org/10.1016/j.jpowsour.2022.232176.
[8] Boyce AM, Cumming DJ, Huang C, Zankowski SP, Grant PS, Brett DJL, et al. Design of scalable, next-generation thick electrodes: opportunities and challenges. ACS Nano 2021;15(12):18624–32. https://doi.org/10.1021/acsnano.1c09687.
[9] Zheng J, Xing G, Jin L, Lu Y, Qin N, Gao S, et al. Strategies and challenge of thick electrodes for energy storage: a review. Batteries 2023;9(3):151. https://doi.org/10.3390/batteries9030151.
[10] Gastol D, Capener M, Reynolds C, Constable C, Kendrick E. Microstructural design of printed graphite electrodes for lithium-ion batteries. Mater Des 2021;205:109720. https://doi.org/10.1016/j.matdes.2021.109720.
[11] Pfleging W, Pröll J. A new approach for rapid electrolyte wetting in tape cast electrodes for lithium-ion batteries. J Mater Chem A 2014;2(36):14918–26. https://doi.org/10.1039/C4TA02353F.
[12] Huang C, Dontigny M, Zaghib K, Grant PS. Low-tortuosity and graded lithium ion battery cathodes by ice templating. J Mater Chem A 2019;7(37):21421–31. https://doi.org/10.1039/C9TA07269A.
[13] Zhu P, Slater PR, Kendrick E. Insights into architecture, design and manufacture of electrodes for lithium-ion batteries. Mater Des 2022;223:111208. https://doi.org/10.1016/j.matdes.2022.111208.
[14] Saadi MaSR, Maguire A, Pottackal NT, Thakur MSH, Ikram MMd, Hart AJ, et al. Direct ink writing: a 3D printing technology for diverse materials. Adv Mater 2022;34(28):2108855. https://doi.org/10.1002/adma.202108855.
[15] Tagliaferri S, Panagiotopoulos A, Mattevi C. Direct ink writing of energy materials. Mater Adv 2021;2(2):540–63. https://doi.org/10.1039/D0MA00753F.
[16] Zhang M, Mei H, Chang P, Cheng L. 3D printing of structured electrodes for rechargeable batteries. J Mater Chem A 2020;8(21):10670–94. https://doi.org/10.1039/D0TA02099K.
[17] Talens Peiró L, Ardente F, Mathieux F. Design for disassembly criteria in EU product policies for a more circular economy: a method for analyzing battery packs in PC-tablets and subnotebooks. J Ind Ecol 2017;21(3):731–41. https://doi.org/10.1111/jiec.12608.

[18] Reynolds CD, Hare SD, Slater PR, Simmons MJH, Kendrick E. Rheology and structure of lithium-ion battery electrode slurries. Energ Technol 2022;10(10): 2200545. https://doi.org/10.1002/ente.202200545.
[19] Reynolds CD, Lam J, Yang L, Kendrick E. Extensional rheology of battery electrode slurries with water-based binders. Mater Des 2022;222:111104. https://doi.org/10.1016/j.matdes.2022.111104.
[20] Balani SB, Ghaffar SH, Chougan M, Pei E, Şahin E. Processes and materials used for direct writing technologies: a review. Res Eng Des 2021;11:100257. https://doi.org/10.1016/j.rineng.2021.100257.
[21] Ye Z, Chu C, Zhang D, Ma S, Guo J, Cheng Y, et al. Study on 3D-direct ink writing based on adding silica submicron-particles to improve the rheological properties of alumina ceramic ink. Mater Today Commun 2021;28:102534. https://doi.org/10.1016/j.mtcomm.2021.102534.
[22] Cipriani CE, Shu Y, Pentzer EB, Benjamin CC. Viscoelastic and thixotropic characterization of paraffin/photopolymer composites for extrusion-based printing. Phys Fluids 2022;34(9):093106. https://doi.org/10.1063/5.0104157.
[23] Yan J, Huang S, Lim YV, Xu T, Kong D, Li X, et al. Direct-ink writing 3D printed energy storage devices: from material selectivity, design and optimization strategies to diverse applications. Mater Today 2022;54:110–52. https://doi.org/10.1016/j.mattod.2022.03.014.
[24] Bonn D, Paredes J, Denn M, Berthier L, Divoux T, Manneville S. Yield stress materials in soft condensed matter. Rev Mod Phys 2015:89. https://doi.org/10.1103/RevModPhys.89.035005.
[25] M'Barki A, Bocquet L, Stevenson A. Linking rheology and printability for dense and strong ceramics by direct ink writing. Sci Rep 2017;7(1):6017. https://doi.org/10.1038/s41598-017-06115-0.
[26] Design of yield-stress fluids: a rheology-to-structure inverse problem - Soft Matter (RSC Publishing). https://pubs.rsc.org/en/content/articlelanding/2017/sm/c7sm00758b#fig 1 (accessed 2023-03-20).
[27] Beran T, Mulholland T, Henning F, Rudolph N, Osswald TA. Nozzle clogging factors during fused filament fabrication of spherical particle filled polymers. Addit Manuf 2018;23:206–14. https://doi.org/10.1016/j.addma.2018.08.009.
[28] Clarification of the Dispersion Mechanism of Three Typical Chemical Dispersants in Lithium-ion Battery (LIB) Slurry | Elsevier Enhanced Reader. doi:https://doi.org/10.1016/j.partic.2022.11.013.
[29] Zhang W, He X, Pu W, Li J, Wan C. Effect of slurry preparation and dispersion on electrochemical performances of LiFePO4 composite electrode. Ionics 2011;17(5): 473–7. https://doi.org/10.1007/s11581-011-0560-4.
[30] Bui VTNT, Nguyen BT, Renou F, Nicolai T. Rheology and microstructure of mixtures of iota and Kappa-Carrageenan. Food Hydrocoll 2019;89:180–7. https://doi.org/10.1016/j.foodhyd.2018.10.034.
[31] del-Mazo-Barbara L, Ginebra M-P. Rheological characterisation of ceramic inks for 3D direct ink writing: a review. J Eur Ceram Soc 2021;41(16):18–33. https://doi.org/10.1016/j.jeurceramsoc.2021.08.031.
[32] Ouyang L, Wu Z, Wang J, Qi X, Li Q, Wang J, et al. The effect of solid content on the rheological properties and microstructures of a Li-ion battery cathode slurry. RSC Adv 2020;10(33):19360–70. https://doi.org/10.1039/D0RA02651D.
[33] Azad MS, Patel V, Shah N, Sharma T, Trivedi JJ. Extensional rheological measurements of surfactant–polymer mixtures. ACS Omega 2020;5(48):30787–98. https://doi.org/10.1021/acsomega.0c00481.
[34] Rizvi A, Bae SS, Mohamed NMA, Lee JH, Park CB. Extensional flow resistance of 3D fiber networks in plasticized nanocomposites. Macromolecules 2019;52(17): 6467–73. https://doi.org/10.1021/acs.macromol.9b00885.
[35] Schramm, G. A Practical Approach to Rheology and Rheometry.